

A Pre-computed Brain Response Atlas for Instantaneous Strain Estimation in Contact Sports

SONGBAI JI^{1,2} and WEI ZHAO¹

¹Thayer School of Engineering, Dartmouth College, 14 Engineering Drive, Hanover, NH 03755, USA; and ²Department of Surgery and of Orthopaedic Surgery, Geisel School of Medicine at Dartmouth, Hanover, NH 03755, USA

(Received 10 June 2014; accepted 19 November 2014; published online 2 December 2014)

Associate Editor Joel D. Stitzel oversaw the review of this article.

Abstract—Finite element models of the human head play an important role in investigating the mechanisms of traumatic brain injury, including sports concussion. A critical limitation, however, is that they incur a substantial computational cost to simulate even a single impact. Therefore, current simulation schemes significantly hamper brain injury studies based on model-estimated tissue-level responses. In this study, we present a pre-computed brain response atlas (pcBRA) to substantially increase the simulation efficiency in estimating brain strains using isolated rotational acceleration impulses parameterized with four independent variables (peak magnitude and duration, and rotational axis azimuth and elevation angles) with values determined from on-field measurements. Using randomly generated testing datasets, the partially established pcBRA achieved a 100% success rate in interpolation based on element-wise differences in accumulated peak strain (ϵ^p) according to a “double-10%” criterion or average regional ϵ^p in generic regions and the corpus callosum. A similar performance was maintained in extrapolation. The pcBRA performance was further successfully validated against directly simulated responses from two independently measured typical real-world rotational profiles. The computational cost to estimate element-wise whole-brain or regional ϵ^p was 6 s and <0.01 s, respectively, vs. ~ 50 min directly simulating a 40 ms impulse. These findings suggest the pcBRA could substantially increase the throughput in impact simulation without significant loss of accuracy from the estimation itself and, thus, its potential to accelerate the exploration of the mechanisms of sports concussion in general. If successful, the pcBRA may also become a diagnostic adjunct in conjunction with sensors that measure head impact kinematics on the field to objectively monitor and identify tissue-level brain trauma in real-time for “return-to-play” decision-making on the sideline.

Keywords—Traumatic brain injury, Sports concussion, Rotational acceleration, Pre-computation, Dartmouth Head Injury Model.

Address correspondence to Songbai Ji, Thayer School of Engineering, Dartmouth College, 14 Engineering Drive, Hanover, NH 03755, USA. Electronic mail: Songbai.Ji@Dartmouth.edu

INTRODUCTION

Sports-related concussion is a major public health and socio-economical problem in the United States estimated to occur in 1.6–3.8 million individuals annually, and is particularly common in football and ice hockey.¹¹ However, concussions are frequently under- or undiagnosed in a competitive athletic environment because signs of cognitive alterations may be mild and masked, unrecognized, or ignored by the athletes.³⁵ Both concussive and subconcussive head impacts have been associated with acute brain injury as well as chronic neurodegeneration.³⁶ Growing evidence suggests that a substantial group of athletes without clinically diagnosed concussion also exhibits measurable neurocognitive and neurophysiological impairment present on diffusion tensor imaging (DTI)^{2,33} and functional magnetic resonance imaging (fMRI).^{6,50} In addition, these athletes experience significantly more impacts, especially to the top-front of the head.^{6,50} A recent study analyzing head impact exposures (HIEs)¹⁵ in a cohort of concussed athletes suggests that those with delayed diagnosis of concussion sustained significantly more impacts on the day and within seven days of injury than those with immediate diagnosis of concussion.³ These studies underscore the importance of the cumulative effects of repetitive head impacts on the risk of concussion and associated neurodegeneration.

To better understand the mechanisms of sports-related concussion, on-field measurements of HIE have provided important insights on the kinematics involved.^{3–5,15} Various kinematics-based injury metrics have been proposed to assess the risk of concussion, including the head injury criterion (HIC), a generalized acceleration model for brain injury threshold (GAMBIT),³⁹ head impact power (HIP),⁴⁰ and the HIT

severity profile (HITsp).¹⁷ Because many believe rotational acceleration to be a primary mechanism for diffuse axonal injury (DAI), including loss of consciousness and concussion,^{21,27} more recent efforts such as the rotational injury criterion (RIC) and power rotational head injury criterion (PRHIC) based on the HIC and HIP counterparts, respectively,²⁶ and the brain injury criterion (BrIC),⁴⁸ are solely composed of head impact rotational components. These efforts are in-line with the work by Rowson and colleagues who investigated head rotational kinematics as an injury risk function in football,⁴⁵ while later they extended their work by combining both linear and rotational kinematics to assess the probability of concussion.⁴⁴ Despite these efforts, no consensus has been reached on an appropriate kinematics-based injury metric or a concussion tolerance threshold to date. In part, this may be because these injury metrics, alone, do not provide region-specific brain mechanical responses that are presumed to be directly responsible for initiating the injury at the tissue level.

To understand how external energy in head impact is converted into regional brain mechanical responses sufficient to initiate the injury at the microstructural level, finite element (FE) models of the human head play a unique and important role in estimating tissue-level brain mechanical responses such as strain, stress, and pressure that are otherwise infeasible or challenging to obtain in live humans.⁵⁷ For example, several research groups have attempted to establish a concussion threshold based on model-estimated regional brain responses from analyses of reconstructed NFL impacts,^{29,32,59} pedestrian and motorcycle accidents,⁵⁵ and instrumented helmets from collegiate football players.⁴⁹ Recent work evaluating model-estimated strain and strain rate in the corpus callosum also showed promise in correlating regional brain responses directly with longitudinal changes in neuroimaging parameters.³⁴ Further, the consistency between model-estimation and neuroimaging findings was significantly improved in terms of the spatial distribution and group-wise extent of potential white matter damage when using strains along white matter fiber directions instead of isotropic maximum principal strains.^{2,24} Because brain strains are significantly correlated to rotational (\mathbf{a}_{rot}) but not linear (\mathbf{a}_{lin}) acceleration,²⁵ parametric studies have also investigated the significance of \mathbf{a}_{rot} directionality and pulse shapes.^{28,42,54,58}

However, a critical limitation in these head FE models is that they incur a substantial computational cost to simulate even a single head impact (hours on a modern multi-core computer or even a super computer).^{13,23,24,29,41,48,49,59} In large part, therefore, these models have been limited to studies that focus on single head impacts to date, and current FE simulation

schemes are likely impractical to handle the amount of computations to study the cumulative effects of repetitive head impacts especially on a large scale (e.g., hundreds of players where each athlete typically sustains hundreds of impacts in a single season of play).^{3,4,6,52} In addition, the extensive computational cost and demand in high performance computational hardware also significantly hamper the establishment of injury risk metrics based on model-estimated tissue-level mechanical responses such as strain or stress as opposed to global kinematic measures or their variants alone.⁴⁸ A substantial increase in the efficiency in head impact simulation is, therefore, necessary and much desired to address the computational challenges in model-based brain injury studies in order to accelerate the exploration of the mechanisms of traumatic brain injury (sports concussion in particular) in the future.

In this study, we present the concept of a pre-computed brain response atlas (pcBRA) to enable an efficient estimation (within seconds or instantaneously as opposed to hours) of brain strain responses without significant loss of accuracy from the pcBRA estimation itself. Critical to its potential success is the ability to use isolated \mathbf{a}_{rot} alone instead of full degrees-of-freedom (DOFs) head impact as model input to estimate brain strain responses,²⁵ thereby substantially reducing the dimensionality of model input parametric space. Ultimately, the practical utility of the technique depends on a systematic and quantitative comparison of pcBRA-estimated brain strain responses with their counterparts directly simulated from actual full DOFs head impacts. In our current study, however, we focus on assessing the pcBRA performance (accuracy and efficiency) using parameterized or idealized \mathbf{a}_{rot} impulses. An initial evaluation of the pcBRA performance was also conducted using two independently measured typical real-world \mathbf{a}_{rot} profiles as input to gain important confidence of the technique. If successful, the pcBRA could substantially increase the throughput in head impact simulation and, thus, accelerate the exploration of the biomechanical mechanism of sports-related concussion.

METHODS

The Dartmouth Head Injury Model (DHIM)

All brain responses were simulated using the recently developed and validated Dartmouth Head Injury Model (DHIM; Fig. 1).^{24,25} Briefly, the DHIM was created with high mesh quality and geometrical accuracy based on high-resolution magnetic resonance images (MRI) of an athlete. When neuroimaging is available for other individuals, the DHIM also allows the creation of a geometrically accurate subject-specific

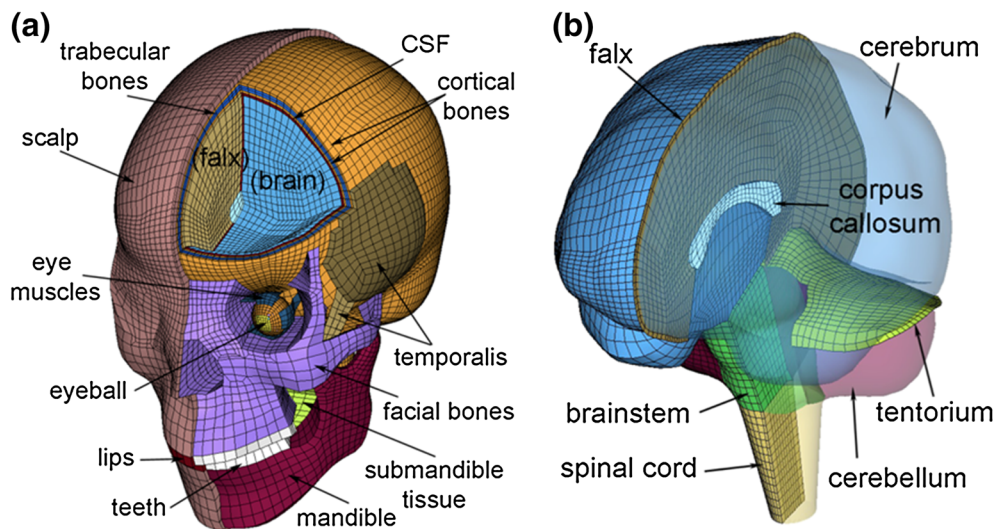


FIGURE 1. The DHIM with color-coded regions of interest showing the head exterior (a) and intracranial components. (b) The model includes part of the spinal cord to improve its biofidelity in the inferior region, which was excluded from analysis in this study.

head FE model. The DHIM is composed of solid hexahedral and surface quadrilateral elements with a total of 101.4 k nodes and 115.2 k elements (56.6 k nodes and 55.1 k elements) and a combined mass of 4.562 kg (1.558 kg) for the whole head (brain). The average element size for the whole head and the brain is 3.2 ± 0.94 mm and 3.3 ± 0.79 mm, respectively. The material properties for the brain and other head components are reported previously.^{24,25} Because no consensus has been reached on how best to characterize brain material properties and experimental observations conflict on the relative stiffness of grey and white matter,⁵³ the entire brain was modeled as a homogenous medium without incorporating the possible inter-regional differences in material properties or material property anisotropy using a hyperelastic material model identical to the “average model” in Kleiven.²⁹ DHIM achieved an overall “good” to nearly “excellent” validation performance against relative brain-skull displacement and pressure responses from cadaveric impacts,^{19,20,38,51} as well as full-field brain strains in a live human volunteer,⁴⁷ as previously reported.^{24,60}

Reduction in Model Input Parametric Dimension

Conceptually, a head FE model is simply a mathematical function mapping impact kinematic parameters (i.e., time-varying \mathbf{a}_{lin} and \mathbf{a}_{rot} accelerations relative to the head center of gravity, CG) into regional brain mechanical response variables such as strain, stress and pressure as well as their derivatives either for an individual element or a specific region of interest (ROI; e.g., the entire white matter, the cerebrum, or the

corpus callosum). The functional mapping for a response distribution within the FE domain is abstracted as the following equation:

$$\mathbf{F} = \mathbf{F}(\mathbf{a}_{lin}, \mathbf{a}_{rot}), \quad (1)$$

where the model-specific function, \mathbf{F} , is composed of material properties of various components, interfacial boundary conditions, meshes, element formulations, and numerical simulation solver, etc. Because a given head impact leads to a unique set of output responses, \mathbf{F} is deterministic; thus, allowing a set of brain responses to be *pre-computed* by systematically varying the input parameters to build a “library” or “look-up table” to enable a highly efficient “interpolation” for brain response estimates using solutions already computed. A similar pre-computation strategy has already been successfully employed in image-guided neurosurgery,¹⁶ but has not been applied in brain dynamic simulations before. A brute-force approach is likely infeasible here because of the input’s high dimensionality (a total of 12 DOFs since each component of the 6-DOFs accelerations can be an independent function of time) in head impact that would require an exponential computational complexity of $O(M^N)$, where N and M are the number of parametric dimensions and the number of samples along each dimension, respectively. Therefore, reduction in the dimension of model input parametric space or the number of independent variables required to pre-compute the response atlas is *essential*.

It is well known that brain strain responses are significantly correlated to \mathbf{a}_{rot} but not to \mathbf{a}_{lin} ^{23,29,49,59} Using two independently established and validated head FE models, the DHIM and SIMon, brain

strain-related responses (strain, strain rate and stress) are found to be significantly correlated to both the magnitude and duration of \mathbf{a}_{rot} , but not to \mathbf{a}_{lin} ,²⁵ because of brain's high bulk modulus. These results establish the feasibility of using isolated \mathbf{a}_{rot} -only to estimate brain strain responses, \mathbf{F}_{strain} , without significant loss of accuracy. Therefore the following functional mapping is obtained that effectively halves the number of parametric dimensions required to establish the brain strain response atlas:

$$\mathbf{F}_{strain} \approx \mathbf{F}(\mathbf{a}_{rot}). \quad (2)$$

Further reduction in the parametric dimension is necessary and possible because the temporal characteristics of on-field head impacts are similar where a single largest acceleration peak dominates (typically with much smaller secondary peaks) and is similar to a triangular waveform.^{9,10} Using the largest rotational acceleration peak, \mathbf{a}_{rot} can be parameterized with four independent variables including its peak magnitude (a_{rot}^p) and duration (Δt), as well as the azimuth and elevation angles, θ and α , characterizing the instantaneous rotational axis, Ω . In practice, Ω is determined by the \mathbf{a}_{rot} components along the three major axes when the resultant a_{rot}^p is reached. The strain response functional mapping is re-written into:

$$\mathbf{F}_{strain} \approx \mathbf{F}(\mathbf{a}_{rot}) = \mathbf{F}_1(a_{rot}^p, \Delta t, \theta, \alpha) + \mathbf{F}_{err}, \quad (3)$$

where \mathbf{F}_1 is the response from the parameterized \mathbf{a}_{rot} symbolizing a 1st-order approximation, while \mathbf{F}_{err} is the residual error representing the element-wise difference distribution between pcBRA-estimated responses and the ground-truth directly from the full DOF \mathbf{a}_{rot} . In sum, these idealization and parameterization of \mathbf{a}_{rot} allows using four instead of as many as 12

DOFs to generate model inputs, which is the basis of the pre-computation in this study.

Rotational Axis Sampling Space

The rotational axis sampling space can be further halved because of the head geometrical symmetry relative to the mid-sagittal plane (i.e., xz -plane in Fig. 2a). For a given $\Omega(\theta, \alpha)$ passing through the head CG, the head rotates counter clock-wise (CCW) by convention. A clock-wise (CW) rotation with an identical magnitude temporal profile with respect to the xz -plane mirroring axis, $\Omega'(-\theta, \alpha)$, or equivalently, a CCW rotation with respect to the its negative axis, $\Omega''(180^\circ - \theta, -\alpha)$, produces a symmetric brain response relative to the mid-sagittal plane compared to that using Ω as the rotational axis. When Ω traverses through the shaded hemisphere shown in Figs. 2b and 2c, Ω' traverses through the other un-shaded hemisphere. In combination, therefore, Ω and Ω' sample the entire rotational axis parametric space.

To further illustrate the rotational axis sampling space, Fig. 3 shows pairs of rotational axes that produce mirroring or symmetric brain responses when the head is subjected to rotational impulses of an identical magnitude temporal profile. The shaded hemisphere in Figs. 2b and 2c corresponds to the shaded area in Fig. 3 (i.e., area defined by θ range $[-90^\circ, 90^\circ]$ and α range $[-90^\circ, 90^\circ]$; including the boundary). For a rotational axis in the unsampled region (e.g., Ω'' and Ω''' in Fig. 3), the brain responses can be easily obtained by mirroring the responses from the corresponding rotational axis in the sampled region (e.g., Ω and Ω' , respectively, in Fig. 3) about the mid-sagittal plane.

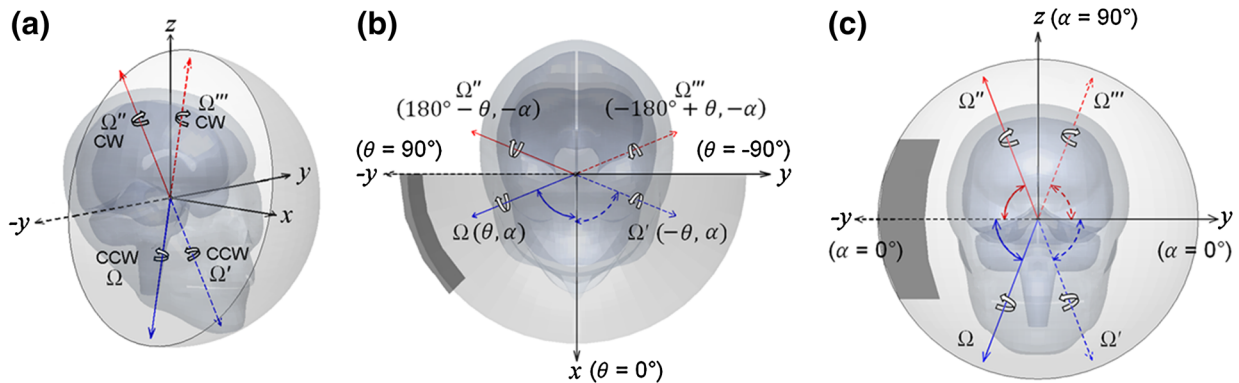


FIGURE 2. Schematic of head rotational axes and the sampling space in iso- (a), top (b), and frontal (c) views. Brain responses using Ω and Ω' (solid), or Ω'' and Ω''' (dashed), as the rotational axes are symmetric about the mid-sagittal or xz -plane. When Ω traverses through the shaded hemisphere, its counterpart, Ω' , traverses through the other un-shaded hemisphere. In combination, they sample the entire rotational axis parametric space. The dark area corresponds to the same identified parametric space in Fig. 3.

Generation of pcBRA for Brain Strain Responses

Triangulated \mathbf{a}_{rot} -only impulses parameterized by four independent variables, $a_{rot}^p, \Delta t, \theta,$ and $\alpha,$ were generated as model inputs by combining selected values of each variable with their respective ranges determined from on-field measurements. Because higher a_{rot}^p values are likely more relevant to potential injury but occur less frequently,^{7,43} we have constrained a_{rot}^p to 1500–4500 rad/s,² or approximately between the 50th and the 95th percentile of a_{rot}^p in on-field ice-hockey.²³ The lower and upper bounds were also comparable to the 75th percentile subconcussive and (slightly below) the 50th

percentile concussive a_{rot}^p magnitudes in collegiate football, respectively (Fig. 4).⁴⁵ The range of the impulse duration, $\Delta t,$ was based on the temporal characteristics of high school football on-field measurements (mean plus and minus twice the standard deviation according to the reported duration of 10 ± 3 ms for \mathbf{a}_{lin}),⁸ which encompassed the average \mathbf{a}_{lin} impact duration of 14 ms reported in collegiate football.⁴³ The full ranges of θ and α were both $[-90^\circ, 90^\circ],$ as explained earlier (Fig. 3). To further limit the amount of computation in this study, they were restricted to $[45^\circ, 90^\circ]$ and $[-30^\circ, 30^\circ],$ respectively (dark area in Fig. 3), effectively

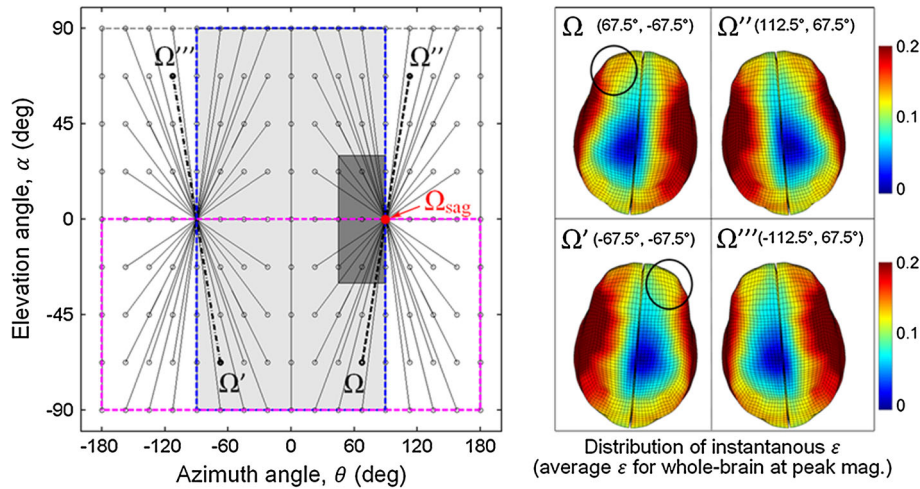


FIGURE 3. Schematic of head rotational axis sampling space (left). Each pair of sampling points connected by a line segment generates brain responses symmetric about the mid-sagittal plane when using an identical resultant \mathbf{a}_{rot} profile. Brain strain responses in deformed states are shown for two pairs of rotational axes (right). Symmetric responses about the mid-sagittal plane were evident for those generated by Ω and Ω'' , and by Ω' and Ω''' , respectively. However, responses generated by Ω and Ω' , and by Ω'' and Ω''' , were not (see circled regions). Both the shaded area (θ range $[-90^\circ, 90^\circ]$ and α range $[-90^\circ, 90^\circ]$) and the lower half bounding box (θ range $[-180^\circ, 180^\circ]$ and α range $[-90^\circ, 0^\circ]$) can be used to sample half of the parametric space (the former was chosen in this study, which is identical to the shaded hemisphere in Fig. 2).

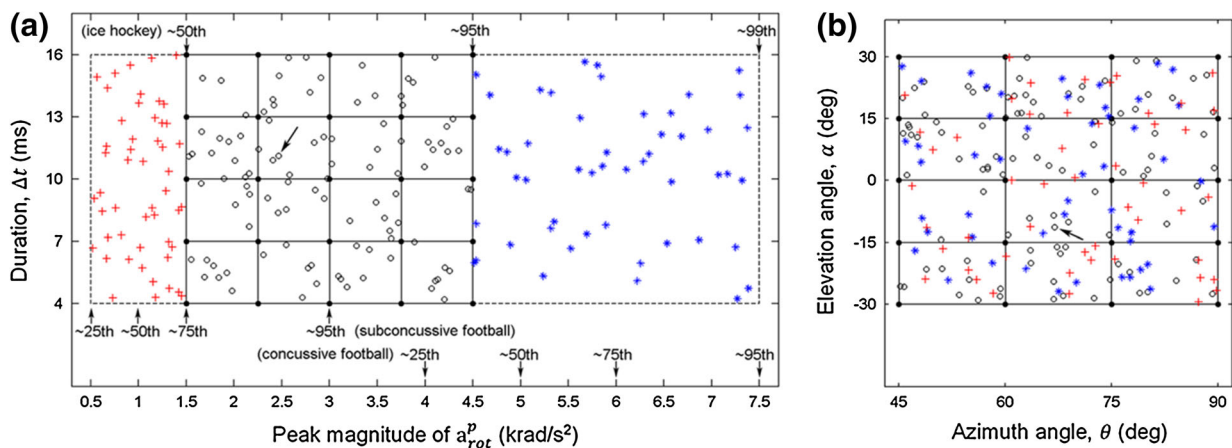


FIGURE 4. Distribution of the training (black dots) and testing (circles, crosses and stars for in-range interpolation and below- and above-range extrapolation, respectively) datasets as orthogonal 2D projections of the 4D data points on the $a_{rot}^p - \Delta t$ (a) and $\theta - \alpha$ planes (b). Locations for representative a_{rot}^p values that approximately correspond to characteristic on-field measurements are also shown. Kinematic variable values for one representative interpolation testing data point are: $a_{rot}^p = 2647.1$ rad/s², $\Delta t = 11.1$ ms, $\theta = 66.9^\circ$, $\alpha = -11.4^\circ$ (arrows).

simulating rotational impulses near a sagittal rotation corresponding to (oblique) frontal impacts in the parametric space. The empirically determined range, step size, and the number of samples for each variable are summarized in Table 1. Combining each unique value for each individual variable, a total of 500 ($5 \times 5 \times 4 \times 5$) rotational impulses were generated to serve as the pcBRA training dataset, which effectively formed a four-dimensional (4D) regular grid data structure (their orthogonal two-dimensional (2D) projections are shown in Fig. 4).

For all parameterized \mathbf{a}_{rot} impulses, an additional 25 ms zero acceleration was appended to ensure reaching brain peak responses in simulation; Fig. 5). The resulting \mathbf{a}_{rot} profile was used to simulate a rigid skull rotation about the given axis passing through the head CG (the skull, scalp and face were all simplified as rigid bodies). Maximum principal engineering strain (ϵ ; Abaqus output variable “NEP”) was extracted for each brain element at every temporal point (resolution of 1 ms) to obtain the peak value (ϵ^p) regardless of the time of occurrence.

Performance Evaluation Using Idealized \mathbf{a}_{rot}

Interpolation

A testing dataset of 100 rotational impulses were created by randomly generating values for each indi-

TABLE 1. Summary of the rotational impulse parameterization variables and their ranges, step sizes and numbers of samples used to establish the pcBRA.

Variable	a_{rot}^p (rad/s ²)	Δt (ms)	θ (deg)	α (deg)
Range	[1500, 4500]	[4, 16]	[45, 90]	[-30, 30]
Step size	750	3	15	15
# of samples	5	5	4	5

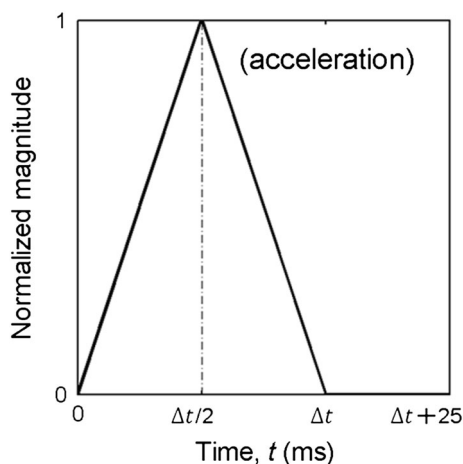


FIGURE 5. The normalized, triangulated head rotational impulse temporal profile (Δt range 4–16 ms).

vidual variable within the corresponding range (Table 1) following a uniform distribution and then randomly combining them with the generated values (Fig. 4).²⁵ The ground-truth ϵ^p at each element was obtained *via* a direct simulation using each impulse as model input. By comparison, the pcBRA-interpolated ϵ^p was obtained through a multivariate linear interpolation (*via* Matlab function “interp.m”) operated independently for each element using values at neighboring 4D grid points in the atlas.¹⁸ Element-wise absolute differences in ϵ^p were obtained and further normalized by the directly simulated ground-truth counterparts to calculate the relative difference. Because the resulting normalized, element-wise differences constituted a spatial distribution within the FE domain, we reported the volume fractions of brain experiencing ϵ^p element-wise differences relative to the directly simulated ground-truth above a range of percentage levels (varied from 0 to 100% at a step size of 1%) to characterize their response differences.

The normalized differences relative to the ground-truths, alone, however, did not necessarily reflect any clinical significance relative to injury-causing thresholds (e.g., the relative difference could be large in percentage but its magnitude may be sufficiently small and clinically irrelevant).²⁵ Therefore, the element-wise response differences were further normalized by a range of injury thresholds (0.05–0.25 with a step size of 0.05) to evaluate their relative differences against each injury threshold values for potential real-world injury risk assessment. The range selected virtually encompassed thresholds established from an *in vivo* animal study (Lagrangian strain range 0.09–0.28 with an optimal threshold of 0.18, or equivalently, engineering strain range 0.086–0.249 with an optimal threshold of 0.166)¹ and FE-based analyses of real-world injury cases (e.g., 0.19 in the grey matter,⁵⁹ 0.21 (0.26) in the corpus callosum (grey matter).²⁹ Similarly, we reported the volume fractions above a range of percentage differences for each injury threshold.

For each testing rotational impulse evaluated, we defined that the pcBRA-interpolated response was sufficiently accurate when the volume fraction of large element-wise differences in ϵ^p (i.e., >10% relative to the ground-truth or a given injury threshold) for the whole-brain was less than 10% (dubbed the “double-10%” criterion). A success rate as the percentage of the testing impulses for which the pcBRA-interpolation was sufficiently accurate was used to evaluate the overall pcBRA interpolation accuracy.

Finally, because tissue-level regional responses can be conveniently used to assess region-specific risk of injury for a given ROI,^{29,49,59} we also computed the volume-weighted regional average ϵ^p for generic brain regions (whole-brain, cerebrum, cerebellum and

brainstem) and the corpus callosum to evaluate the pcBRA estimation performance. Similarly, the pcBRA estimate was considered sufficiently accurate when the absolute difference between the pcBRA-estimated response and the ground-truth was within 10% relative to the ground-truth or the same range of injury thresholds. Analogously, a success rate was used to assess the overall pcBRA performance in regional response estimate.

Extrapolation

Because the training dataset input variables were constrained within their ranges (Table 1) and did not encompass the entire sampling space, it was necessary to evaluate the pcBRA extrapolation performance. This was especially true for a_{rot}^p because only a relatively small range of on-field measurements (50–95th percentile values in on-field ice hockey; Table 1) was covered. We did not evaluate the extrapolation performance for other variables because for Δt , twice the standard deviation covered approximately 95.4% of occurrences (assuming a normal distribution). Although θ and α were also restricted to a small range, they were intentionally limited and could easily be expanded to cover the entire sampling space in the future.

Two separate testing datasets ($N = 50$ each) were randomly generated by constraining a_{rot}^p to a range either immediately below (500–1500 rad/s²) or above (4500–7500 rad/s²) that in the training dataset (Fig. 4) while maintaining the same ranges for other variables using the same approach described previously. The lower and upper end of a_{rot}^p for the below- and above-range extrapolation approximately corresponded to the 25th percentile subconcussive and the 95th percentile concussive a_{rot}^p values for collegiate football, respectively (Fig. 4).⁴⁵ Element-wise whole-brain strain responses were obtained *via* a spline-based extrapolation (*via* Matlab function “interp.m”) using values at neighboring grid points in the pcBRA.¹⁸ Similarly, we computed the volume fractions above a range of percentage differences in ε^p relative to the directly simulated ground-truth and the same range of injury thresholds, and further reported the success rates based on the “double-10%” criterion. In addition, the success rates for pcBRA-extrapolated regional strain responses for generic regions and the corpus callosum were also reported.

Performance Evaluation Using Two Typical Real-World \mathbf{a}_{rot} Profiles

The pcBRA performance was further assessed by comparing against the directly simulated results using two typical \mathbf{a}_{rot} profiles independently measured from anthropomorphic test device (ATD) as inputs.^{10,46}

Because only the resultant profiles were available, mono-axis sagittal rotations were simulated using the corresponding entire \mathbf{a}_{rot} profile (Ω_{sag} in Fig. 3). By comparison, the major \mathbf{a}_{rot} peak was parameterized into a triangular impulse by maintaining an identical rotational velocity, v_{rot}^p , and Δt resulting from the corresponding major peak, as detailed in Fig. 6 for the two profiles. The resulting parameterized impulses were used to interpolate element-wise ε over time as well as ε^p from the pcBRA. Similarly, we reported the element-wise ε^p differences and whole-brain average as a function of time between the two brain responses for each \mathbf{a}_{rot} profile.

Significance of \mathbf{a}_{rot} Parameterization Impulse Shape

Our pcBRA was established based on triangulated \mathbf{a}_{rot} impulses. To investigate the significance of \mathbf{a}_{rot} parameterization impulse shape, a sine and a haversine impulse resulting in an identical v_{rot}^p (of 15 rad/s) from a typical triangular impulse ($a_{rot}^p = 3000$ rad/s², $\Delta t = 10$ ms) were further generated as model inputs to simulate a sagittal rotation (Ω_{sag} in Fig. 3). The resulting ε^p was similarly compared against that from the triangular impulse.

Data Analysis

For all simulations, brain strain responses were obtained from the DHIM with the given \mathbf{a}_{rot} profile as model input *via* Abaqus/Explicit (Version 6.12; Dassault Systèmes, France). The typical runtime for a 40 ms impulse was ~50 min on a multi-core Linux cluster using 8 CPUs with available Abaqus tokens (Intel Xeon X5560, 2.80 GHz, 126 GB memory). Element-wise ground-truth ε^p was obtained for each impulse simulated. Element-wise ε^p and regional average ε^p for generic brain regions and the corpus callosum were also interpolated or extrapolated using the pcBRA. With 12 CPUs executing in parallel, the computational cost to estimate an element-wise ε^p and a regional average ε^p for one impulse was 6 s and <0.01 s, respectively. All data analyses were performed in MATLAB (R2014a; Mathworks, Natick, MA).

RESULTS

Performance Using Idealized \mathbf{a}_{rot}

The average volume fraction for the whole-brain at a difference percentage level of 10% in ε^p was calculated for each testing impulse relative to either the ground-truth or a range of injury thresholds to

compute an average and a range for the corresponding interpolation or extrapolation testing dataset. Regardless of the normalization denominator, the pcBRA in-range interpolation had a 100% success rate. When normalized by the ground-truths, an 80% success rate was achieved for the below-range extrapolation, and it was nearly 100% for the above-range extrapolation except for one failed case with the highest v_{rot} . When normalized by the range of injury thresholds, higher success rates were achieved at larger injury thresholds, as expected. The below-range extrapolation achieved a 100% success rate except at the lowest threshold of 0.05. For the above-range extrapolation, however, the accuracy performance depended on the magnitude of a_{rot}^p as nearly a 100% success rate was achieved when a_{rot}^p was low even at the lowest threshold (only one case failed), while it significantly degraded when a_{rot}^p was high (Table 2). At the largest threshold of 0.25, however, all above-range extrapolations achieved a 100% success rate.

Whole-brain volume fractions for response differences exceeding the full range of percentage difference levels (0–100%) are shown in Figs. 7, 8, and 9 when normalized by either the ground-truths or the range of injury thresholds for pcBRA in-range interpolation, below- and above-range extrapolations, respectively.

To investigate the location where large relative differences occurred, a Pearson correlation test between the element-wise differences in ε^p relative to the directly simulated ground-truth and the ground-truth ε^p , itself, was performed for all impulses. We found a consistently significant negative correlation between the two

(average correlation coefficient of -0.165 (range -0.077 to -0.344); $p < 0.0001$), suggesting that large differences mostly occurred in regions with low ε^p responses.

A representative impulse was chosen to visually compare the magnitude and distribution of the ground-truth ε^p and the nearly identical pcBRA-interpolated counterpart (Fig. 10, top panel). The responses at the 16 (2^4) neighboring grid points are also shown, which essentially provided the response “modes” for interpolation (Fig. 10, bottom panel).

The pcBRA-estimated regional average ε^p achieved a 100% success rate regardless of the normalization denominator or ROI except when a_{rot}^p was more than 1 krad/s^2 larger than the upper bound in the training dataset (Fig. 11). When normalized by the ground-truth, a 100% success rate was achieved even for the highest a_{rot}^p regardless of the ROI. However, when normalized by the injury thresholds, the success rate degraded especially for larger a_{rot}^p , although a 100% success rate was still maintained at threshold levels ≥ 0.2 .

Performance Using Typical Real-World \mathbf{a}_{rot} Profiles

The pcBRA-estimated ε^p magnitude and distribution were nearly identical to those generated from the “ground-truth” ε^p obtained directly from the simulation using each given \mathbf{a}_{rot} profile as input (Figs. 12, 13; top panels). The nearly identical ε^p response was further confirmed by the volume fraction of their whole-brain ε^p differences (volume fraction of 1.80 and 1.31% at a difference percentage level of 10%; Figs. 12c, 13c) and the nearly identical whole-brain average ε peak values (circled regions in Figs. 12d, 13d).

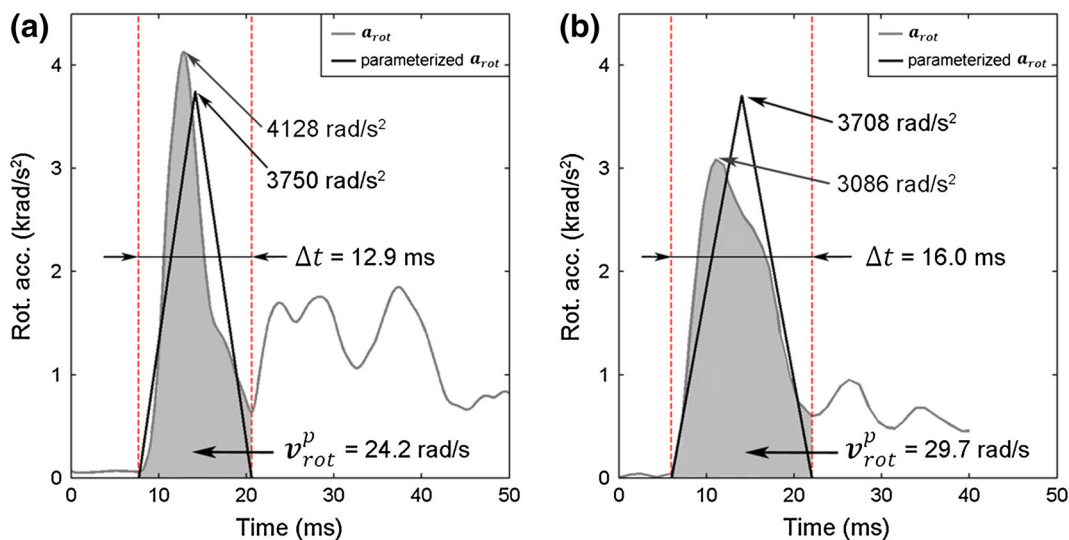


FIGURE 6. Parameterization of two independently measured typical real-world resultant \mathbf{a}_{rot} profiles into triangular impulses (dark lines) by maintaining an identical v_{rot}^p and Δt determined from the corresponding major peak (shaded area). Note that the parameterized a_{rot}^p values in (a)¹⁰ and (b)⁴⁶ were 9.2% lower and 20.2% higher than the corresponding measured counterparts, respectively. Although the measured a_{rot}^p in (b) was 25.2% lower than that in (a), its v_{rot}^p was 22.7% higher.

TABLE 2. Summary of the average and range of volume fractions (VF) for element-wise differences relative to the ground-truths and a range of injury thresholds at the 10% difference level for pcBRA in-range interpolation and below- and above-range extrapolations, together with the corresponding success rates based on the “double-10% criterion”.

Normalization denominator	Injury thresholds						
	Ground-truths	0.05	0.1	0.15	0.2	0.25	
Interpolation ($N = 100$)	Avg. VF (%) VF range (%) Success rate (%)	3.19 0.00–5.99 100	2.65 0.00–8.85 100	0.65 0.00–3.63 100	0.20 0.00–1.48 100	0.00 0.00–0.64 100	0.00 0.00–0.29 100
Below-range extrapolation ($N = 50$)	Avg. VF (%) VF range (%) Success rate (%)	6.22 0.00–28.89 80	1.08 0.00–13.44 96	0.06 0.00–0.99 100	0.00 0.00–0.09 100	0.00 0.00–0.01 100	0.00 0.00–0.00 100
Above-range extrapol.	4.5–5.5 krad/s ² ($N = 16$)	3.24 0.00–5.21 100	5.55 0.21–10.16 93.75	1.76 0.00–4.29 100	0.63 0.00–1.96 100	0.23 0.00–0.86 100	0.00 0.00–0.32 100
	5.5–6.5 krad/s ² ($N = 18$)	4.56 0.84–8.39 100	21.49 2.06–55.99 38.90	5.47 0.28–22.32 94.40	1.98 0.00–6.40 100	0.95 0–3.17 100	0.47 0–1.85 100
	6.5–7.5 rad/s ² ($n = 16$)	6.94 2.61–13.2 93.75	54.24 6.75–89.18 12.50	28.67 1.40–67.48 37.50	13.89 0.35–43.49 43.75	6.00 0.05–22.21 81.25	2.41 0.01–9.83 100

The above-range extrapolation was sub-divided into three groups based on a_{rot}^p to better categorize the pcBRA performance.

Significance of \mathbf{a}_{rot} Parameterization Impulse Shape

The three \mathbf{a}_{rot} profiles (Fig. 14a) of an identical v_{rot}^p and Δt led to nearly identical ε^p responses (a volume fraction of 0.19% (2.76%) exceeded a 5% difference percentage level when comparing ε^p from the sine (haversine) impulse relative to that from the triangular impulse; Fig. 14b), which was further confirmed by their nearly identical ε^p magnitudes and distributions (Fig. 14c).

DISCUSSION

A substantial increase in head impact simulation efficiency is likely critical to ultimate deploy computational models of the human head for large-scale brain injury studies, particularly in contact sports. Using parameterized, triangulated \mathbf{a}_{rot} impulses as training dataset ($N = 500$), we have successfully established a subset of a pre-computed brain response atlas (pcBRA) partially sampling the 4D parametric space based on the DHIM to accurately and efficiently estimate brain strain responses. Using randomly generated in- ($N = 100$), below- ($N = 50$) and above-range ($N = 50$) testing datasets, we have demonstrated excellent pcBRA accuracy performance for element-wise response estimation especially for in-range interpolation as a 100% success rate was achieved based on the “double-10%” criterion regardless of the normalization denominator (directly simulated ground-truths or injury-causing thresholds). An excellent performance (100% success rate) was also achieved when interpolating regional average ε^p for all generic ROIs and the corpus callosum, regardless of the normalization denominator. For extrapolation, excellent or nearly excellent performance was maintained for element-wise or regional average ε^p as long as a_{rot}^p was within 1 krad/s² relative to its bounds in the training dataset, again, regardless of the normalization denominator. The slightly lower success rate for the below-range extrapolation (80%) was likely because of the rather small ε^p due to extreme low a_{rot}^p in input. Even with much higher a_{rot}^p for the above-range extrapolation, excellent or nearly excellent performance was still maintained when normalized by the ground-truth or larger injury-causing thresholds (Table 2). Further, relatively larger element-wise differences were mostly located in regions with low ε^p values (i.e., in corridors along the rotational axes), suggesting more accurate estimates to occur with higher ε^p values that are likely more injury-relevant.

The pcBRA dramatically reduced the computational cost required to achieve element-wise whole-brain responses over that from direct simulation (6 s

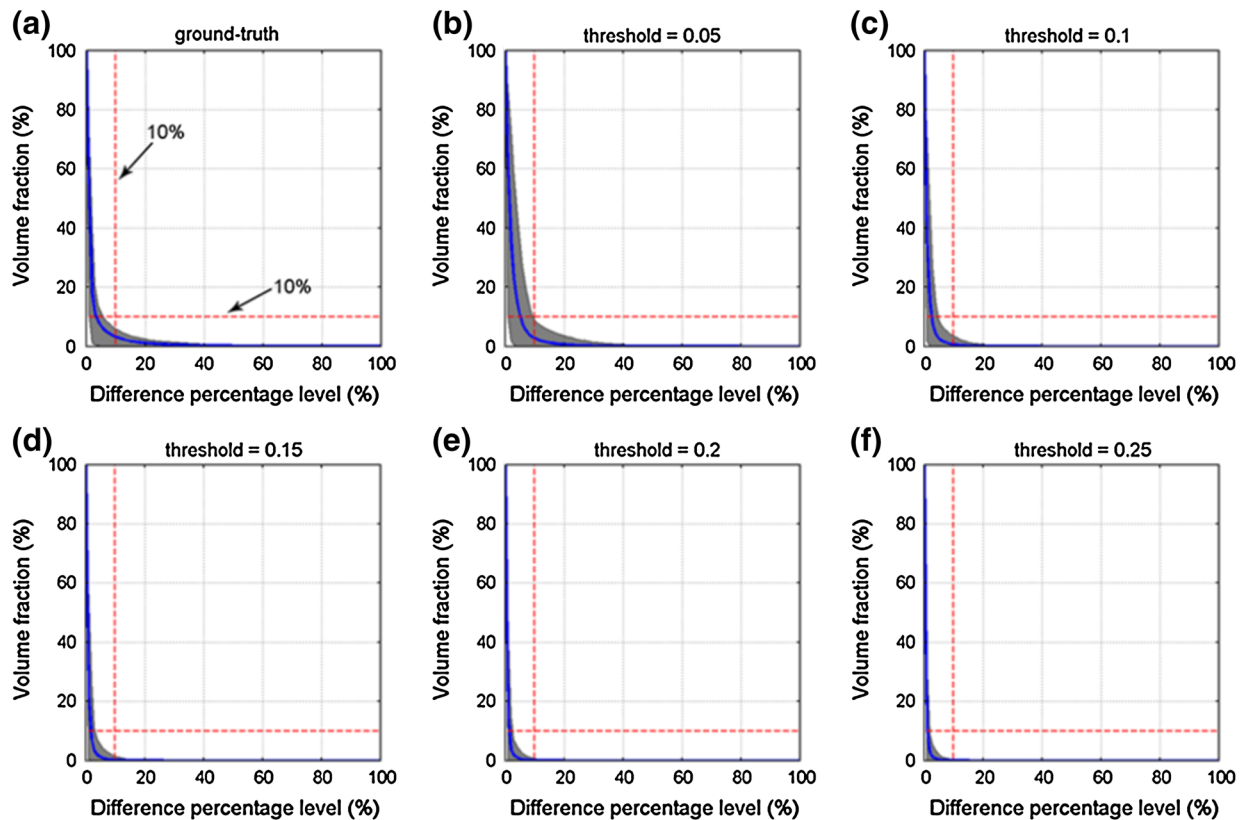


FIGURE 7. Volume fractions for element-wise differences in ε^p relative to the ground-truths and a range of injury thresholds (0.05–0.25) for in-range pcBRA interpolation. Curves and shaded areas represent the average and the range of volume fractions at each difference percentage level for all testing impulses. When normalized by the range of injury thresholds, the volume fractions at each difference percentage level decreased with the increase in the threshold value, as expected.

using 12 CPUs as opposed to ~50 min for a 40 ms impulse using 8 CPUs (the number of CPUs for Abaqus simulation was limited by the available license tokens)). Because regional ε^p values can be pre-computed for any arbitrary ROI (generic or targeted, e.g., corpus callosum) based on the established atlas responses, an instantaneous pcBRA estimate of brain regional strain levels is readily achievable (<0.01 s for each individual interpolation/extrapolation) to assess region-specific injury risk. These results suggest the potential for the pre-computation strategy to substantially increase the throughput in head impact simulation without significant loss of accuracy relative to responses directly simulated from the parameterized impulses. Therefore, the pcBRA could have the capability to enable a large-scale tissue-level, model-based investigation of the mechanisms of traumatic brain injury in the future (e.g., to evaluate brain responses from repetitive head impacts in contact sports).

While it may be possible to reduce FE model simulation time *via* simplified models with coarser meshes, the degradation in solution accuracy is never desirable and is against the general trend of model development. More powerful computers are certainly effective in

reducing simulation time. However, with the ever-growing model sophistication and mesh resolution, the computational challenge persists. Regardless, none of these techniques would be capable of providing an instantaneous regional response in an arbitrary ROI that the pcBRA readily offers, even on a low-end computer. These findings clearly underscore the significant advantages of pcBRA over other conventional, alternative approaches.

Essentially, the pcBRA technique is an end-to-end sampling of a smooth and continuous parametric hyperspace, which has not been applied to brain dynamic simulation before. Additional approximation errors can occur especially for extreme out-of-range extrapolations. While this may seem undesirable, it is critical to consider the utility of model simulation from a system's perspective in a concerted effort (as opposed to an isolated technique by itself) for brain injury studies, especially when (potentially even larger) uncertainties or variations exist in head impact kinematics, neuroimaging, cognitive measures and concussion diagnosis.²⁴ On the other hand, increasing the training dataset sampling density and range (i.e., to avoid “extrapolation”) could easily reduce the

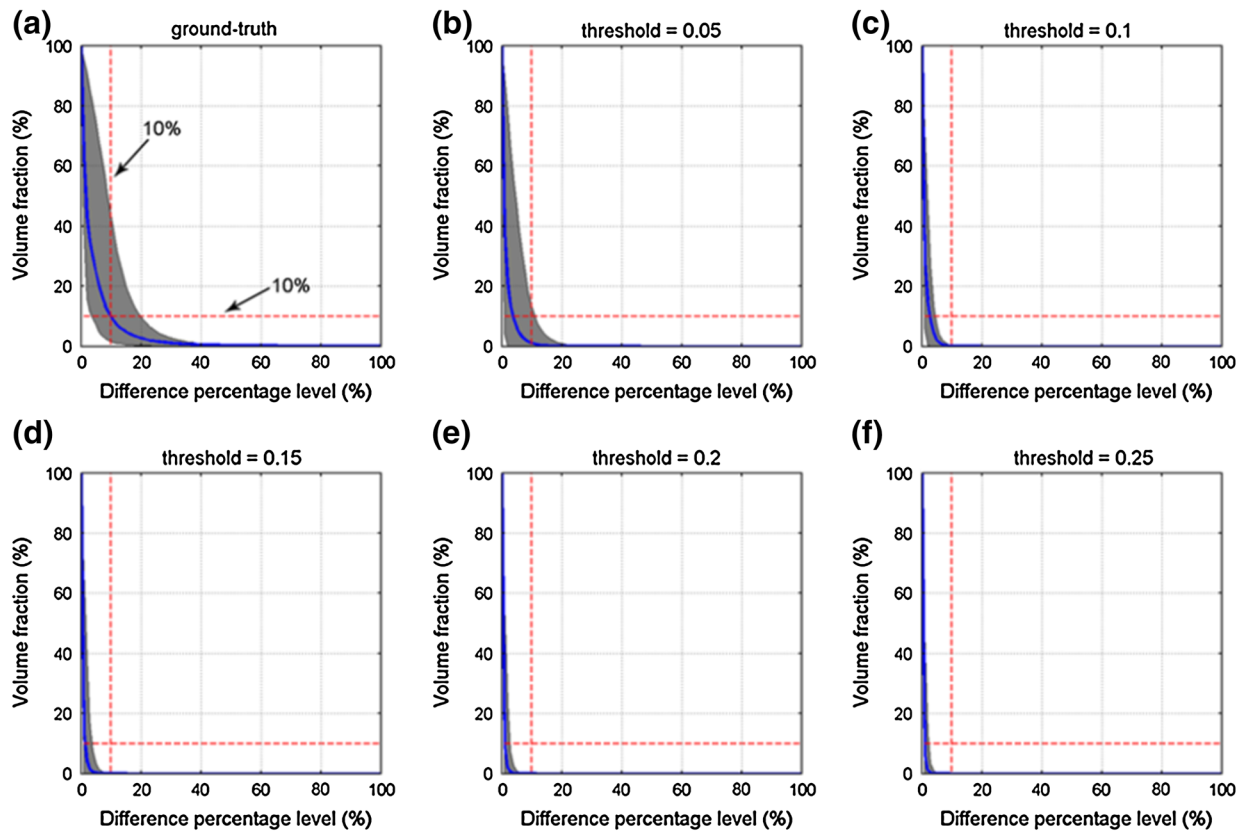


FIGURE 8. Volume fractions for element-wise differences in ε^p relative to the ground-truth and the same range of injury thresholds for below-range pcBRA extrapolation.

unwanted errors. Further, because the accuracy of each simulated pcBRA solution solely depends on the head model, any error in kinematic inputs (e.g., under- or over-estimation of a_{rot}^p or v_{rot}^p) could also be easily compensated for without re-running the pcBRA simulations. These observations highlight the unique scalability of the pcBRA technique.

It must be recognized that the pcBRA feasibility comes at the cost of idealizing full DOFs head impact kinematics into a reduced system by parameterizing the largest single peak of isolated \mathbf{a}_{rot} -only with the minimum number of DOFs (4 as opposed to as many as 12), which would likely result in further loss of accuracy. However, our validations against the directly simulated results using two independently measured typical real-world \mathbf{a}_{rot} profiles suggest that the pcBRA could achieve an excellent performance when simulating mono-axis rotations, which established important confidence of our technique. While subsequent secondary \mathbf{a}_{rot} peaks did influence brain strain response history, they did not significantly alter the peak responses induced by the first major peak (see Figs. 12a, 12b and 13a, 13b for element-wise ε^p and circled regions in Figs. 12d, 13d for whole-brain

average ε peaks). Importantly, because current tissue-level injury metrics including strain, strain rate, their product,²⁷ stress, as well as their variants such as cumulative strain damage measure (CSDM)⁴⁹ are all based on tissue-level accumulated *peak* responses rather than their response *history* during the 40–100 ms impact, the nearly identical element-wise peak strain magnitudes between the pcBRA-estimated and the ground-truth counterparts well justify the use of pcBRA for any real-world, practical application.

The \mathbf{a}_{rot} peak parameterization impulse shape (triangular, sine, or haversine) appears unimportant even when their a_{rot}^p could differ by as much as 21.5% (Fig. 14). As long as they maintain an identical v_{rot}^p and Δt , they lead to almost the same ε^p level. This could be conceptually explained using a dimensional analysis because the transformed brain strain energy is likely proportional to the rotational kinetic energy while they are each proportional to the square of ε^p and v_{rot}^p , respectively.²⁵ Therefore, although the parameterized a_{rot}^p was nearly $\sim 10\%$ lower (Fig. 6a) or 20% higher (Fig. 6b) than the measured counterpart for the two real-world profiles, the pcBRA-estimated and ground-truth ε^p magnitudes and distributions were nearly

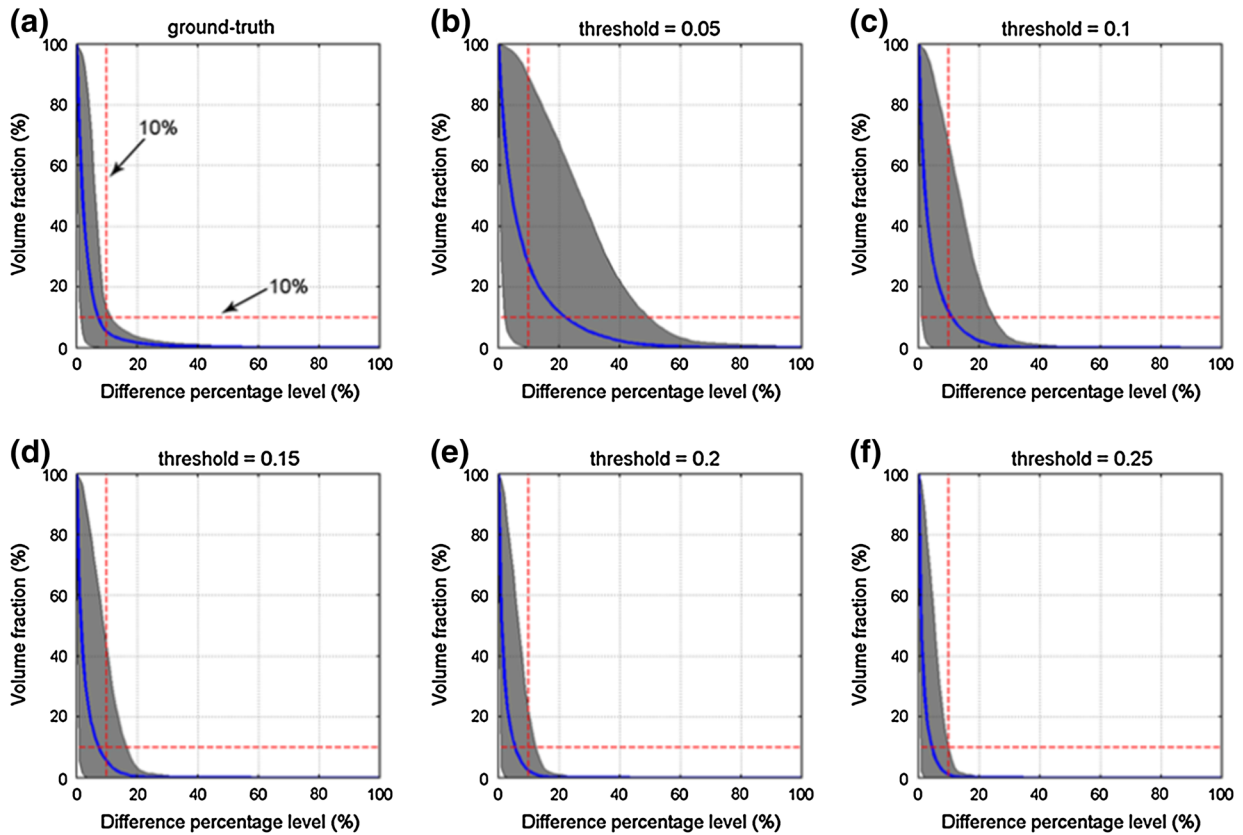


FIGURE 9. Volume fractions for element-wise differences in ε^p relative to the ground-truth and the same range of injury thresholds for above-range pcBRA extrapolation (all testing impulses clustered).

identical (Figs. 12a, 12b; Figs. 13a, 13b). More interestingly, while the measured real-world a_{rot}^p in Fig. 6b was more than 25% lower than that in Fig. 6a, the corresponding v_{rot}^p was nevertheless nearly 23% higher, leading to a $\sim 9\%$ increase in whole-brain average ε^p magnitude (Figs. 12b, 13b). While these findings clearly suggest that v_{rot}^p as opposed to a_{rot}^p may be more informative for injury risk assessment as previously recognized,^{20,25,28,29,48,49,58} a longer Δt lowers ε^p (e.g., whole-brain average ε^p magnitude decreased by more than 15% when Δt was varied from 4 to 16 ms with v_{rot}^p of 25 rad/s), as similarly observed before.²⁸ The decrease in ε^p is likely a result of increased energy dissipation over a longer Δt due to the brain viscoelastic property. Therefore, we have chosen to parameterize a_{rot}^p and Δt separately instead of using v_{rot}^p directly, albeit the latter could allow using three as opposed to four independent variables to establish the pcBRA (and hence, to further significantly reduce the computational cost and atlas storage space).

It should be noted that our current pcBRA performance evaluations were limited to mono-axis, mono-phasic (i.e., acceleration-only) rotations because only resultant \mathbf{a}_{rot} profiles were available.^{10,46} However, a real-world full-DOF \mathbf{a}_{rot} profile could be much more

complicated involving multiple rotational axes in time, or more likely, continuous change of instantaneous rotational axis during impact. In addition, deceleration will inevitably follow the acceleration to avoid an unbounded but unphysical head motion in real world. Parametric studies using multi-axis, multi-phasic impulses would be valuable to gain insights into their significance on brain responses. However, most studies are limited to mono-axis, mono-phasic rotations to-date,^{28,42,54} except for one studying mono-axis, bi-phasic rotations using an idealized 2D model.⁵⁸ Nevertheless, it is important to further investigate the loss of accuracy or the residual error, \mathbf{F}_{err} in Eq. 3, against responses from real-world full-DOF \mathbf{a}_{rot} to assess the pcBRA utility for real-world injury analysis in the future.

Further, when secondary \mathbf{a}_{rot} peaks become increasingly substantial that may violate the assumption of a single major \mathbf{a}_{rot} peak, the pcBRA may become invalid (e.g., some brain regions may experience higher responses at a later time but are not captured). Interesting, the pcBRA in these cases may still serve as an upper- or lower-bound of the true responses (e.g., upper-bound as suggested by a 2D parametric study⁵⁸; albeit, further studies using a

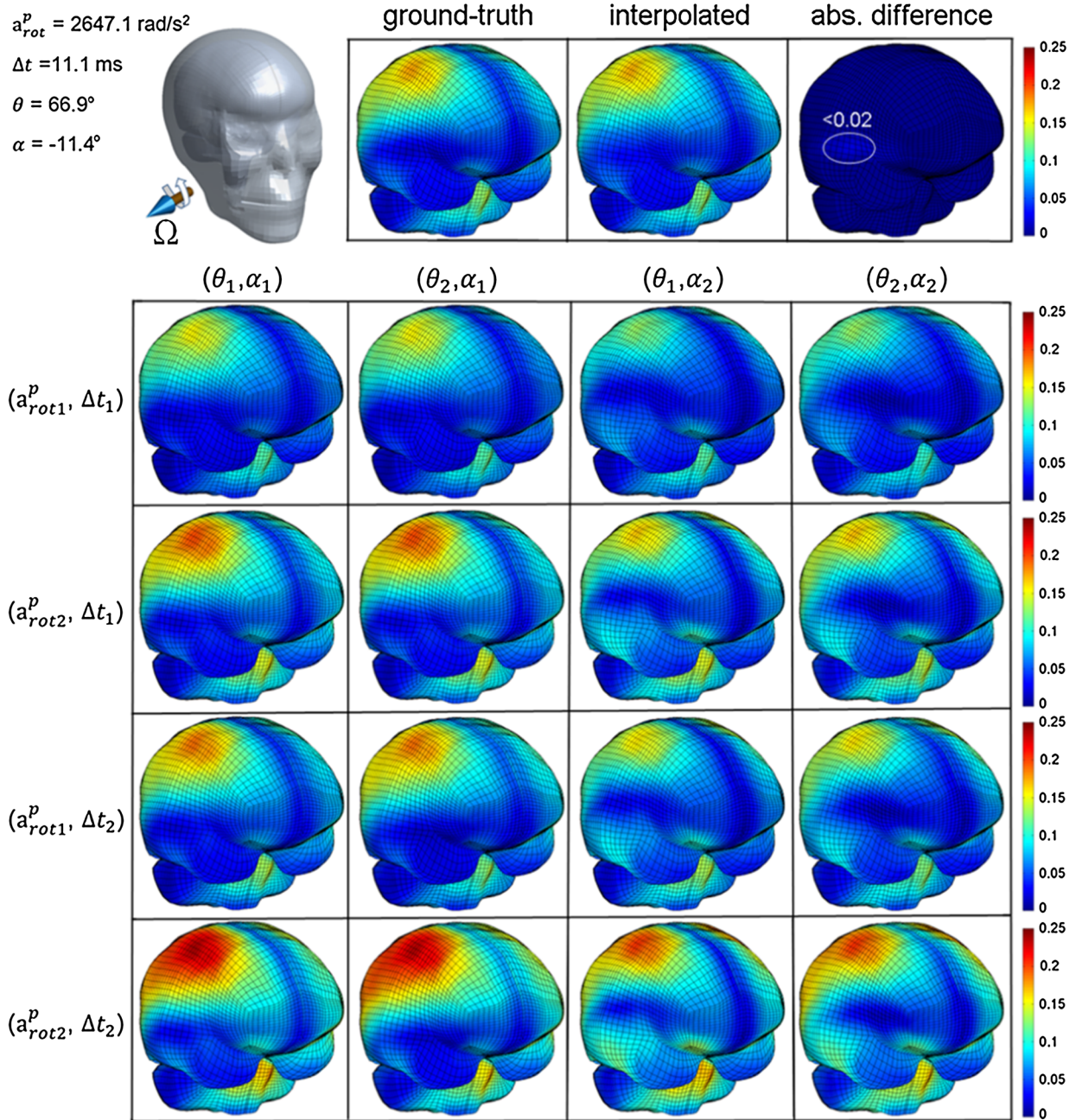


FIGURE 10. Comparison between the pcBRA-interpolated ε^p and the ground-truth from the directly simulated along with their absolute difference (top panel; location for largest differences identified) for a representative rotational impulse in the testing dataset (impulse parameters identified in Fig. 4). The corresponding pcBRA responses at the 16 (2^4) neighboring grid points are also shown (bottom panel; variable values are: $a_{rot1}^p = 2250 \text{ rad/s}^2$, $\Delta t_1 = 10 \text{ ms}$, $\theta_1 = 60^\circ$, $\alpha_1 = -15^\circ$; $a_{rot2}^p = 3000 \text{ rad/s}^2$, $\Delta t_2 = 13 \text{ ms}$, $\theta_2 = 75^\circ$, $\alpha_2 = 0^\circ$). Each row of the 4-by-4 grid represents a comparable response magnitude with an identical v_{rot}^p , while each column represents a similar distribution pattern with an identical rotational axis.

validated and realistic 3D head model are still warranted). It must also be recognized that these rather complicated impact conditions will most likely invalidate other kinematics-based injury metrics as well that similarly focus on a single major \mathbf{a}_{rot} peak. An accurate direct simulation of the true brain strain responses

(peak and history) will inevitably place a more stringent scrutiny on head impact measurement systems that provide the required model input in the first place. These observations, once again, highlight the importance of a concerted effort necessary to elucidate the biomechanical etiology of sports-related concussion.

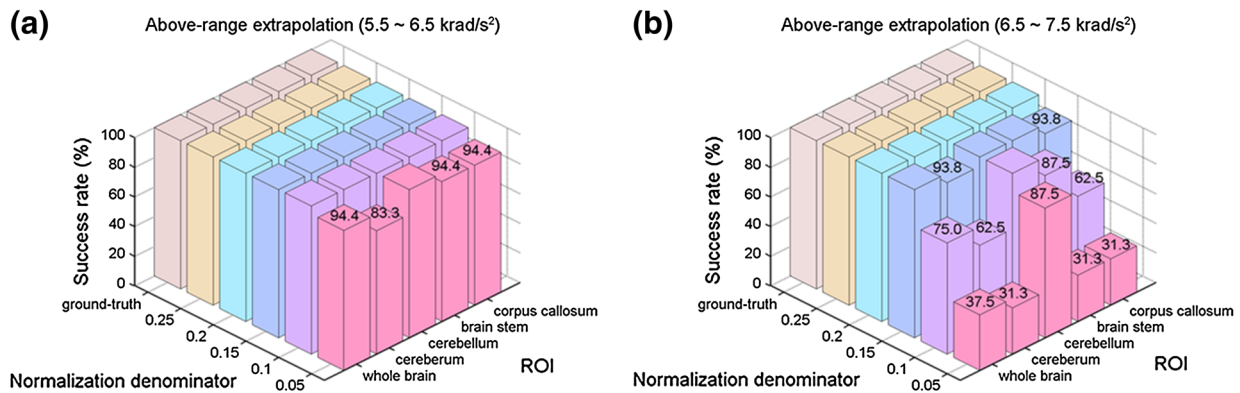


FIGURE 11. The pcBRA success rates for the above-range extrapolation when a_{rot}^p was within (a) 5.5–6.5 krad/s² and (b) 6.5–7.5 krad/s² in terms of regional average ε^p in generic regions and the corpus callosum using a range of normalization denominators. The pcBRA achieved a 100% success rate for all other a_{rot}^p values, and are not shown.

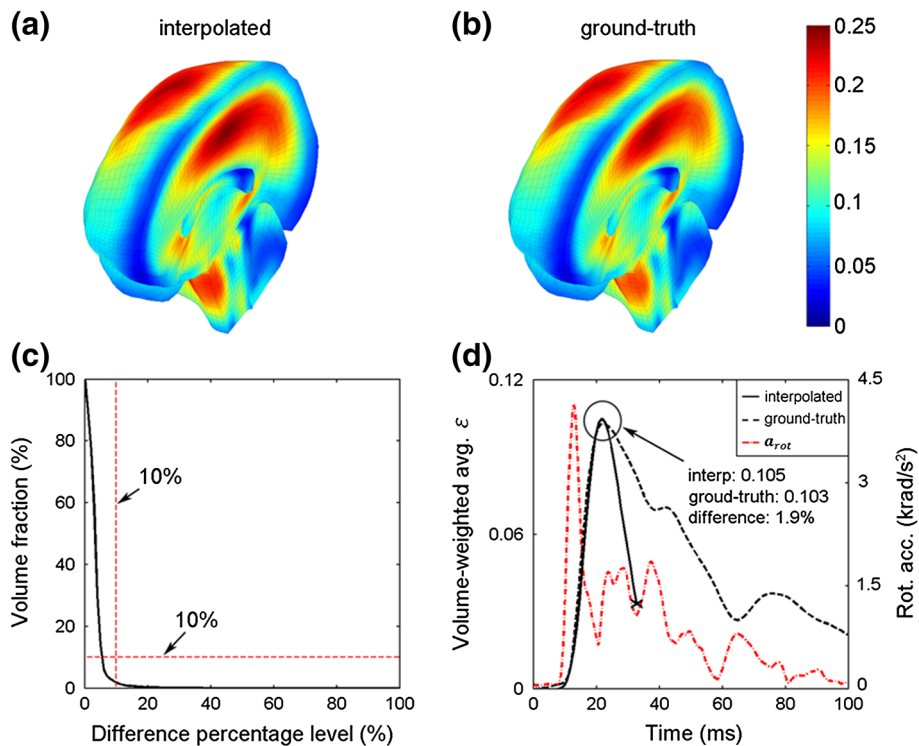


FIGURE 12. Comparison of the (a) pcBRA-estimated and (b) the directly simulated ground-truth ε^p (i.e., element-wise peak responses during the entire impact regardless of time of occurrence) for a typical real-world a_{rot} profile.¹⁰ (c) Volume fractions for ε^p differences relative to the ground-truth. (d) Comparison of volume-weighted whole-brain average ε as a function of time between the pcBRA-estimated and the ground-truth counterpart. The pcBRA-estimated and ground-truth whole-brain ε^p averages in (a) and (b) were 0.116 and 0.114, respectively, which served as upper bounds for the corresponding whole-brain average ε peak values, shown in (d), because not all elements reached their respective peak responses at the same time.

Regardless, to account for these inherent limitations with the pcBRA strategy (i.e., mono-axis, mono-phasic rotations that only capture the single major a_{rot} peak), it is possible to further compensate for F_{err} due to model input idealization and parameterization. However, injecting additional perturbation parameters of the time-varying a_{rot} profile (e.g., mono- vs. biphasic and mono- vs. multi-axis acceleration profile) into the

model input parametric space is perhaps ill-advised because it would necessarily increase the pcBRA computational complexity, exponentially. Instead, it may be advisable to statistically probe the relationship between perturbation in input and variation in response. Analogously, a statistical model could also be used to probe the relationship between model geometrical/anatomical perturbations and variation in

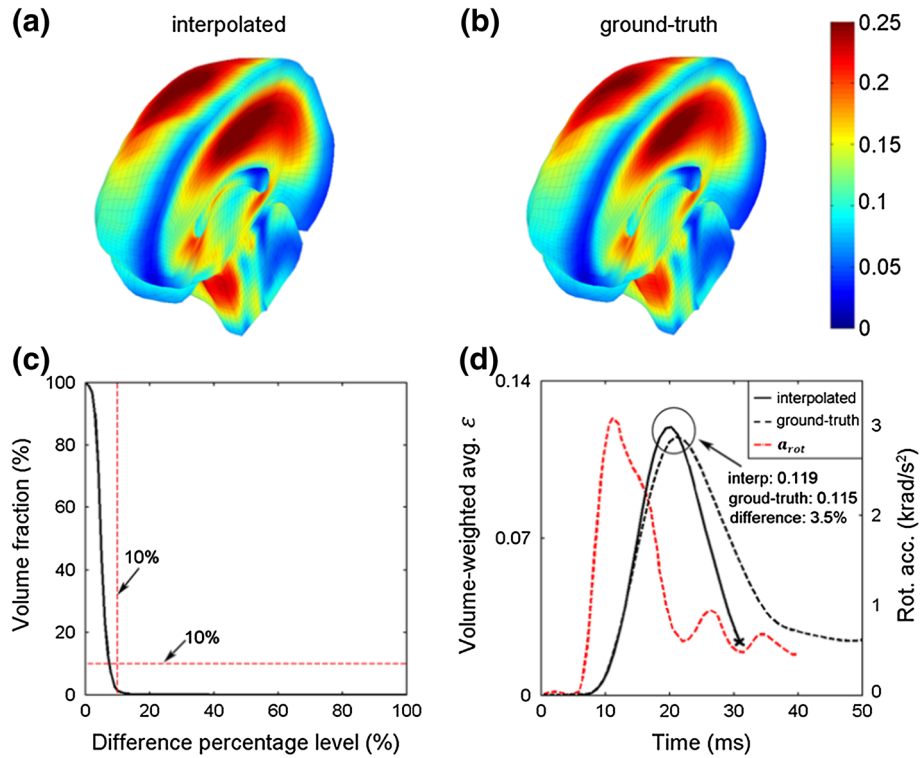


FIGURE 13. A similar comparison between the pcBRA-estimated result and that directly simulated for another independently measured a_{rot} profile (see Fig. 12 for caption).⁴⁴ The pcBRA-estimated and the ground-truth whole-brain ϵ^p averages for this case were 0.130 and 0.124, respectively. Although a_{rot}^p was 25.2% lower than that in Fig. 12, its v_{rot}^p was 22.7% higher, leading to an 8.8% increase in whole-brain average ϵ^p .

response to account for brain individual variability. By statistically quantifying F_{err} in element-wise or regional strain responses (e.g., through a linear regression model),³¹ a higher order and hence, a more accurate approximation of F_{strain} is likely attainable. Additionally, individualized pcBRA could also be established if so desired using subject-specific models that can be developed with existing techniques.^{22,24}

Despite these accuracy concerns, because the pcBRA instantly provides regional tissue-level brain strain responses that are presumed to be directly responsible for initiating region-specific injury, even the 1st-order approximation appears to be a significant step forward in investigating the mechanisms of sports concussion as compared to other studies using isolated d_{lin}^p and/or d_{rot}^p , alone, for injury risk assessment that do not otherwise incorporate regional brain mechanical responses.^{3,4,7,44,45,52} Because it is possible to compare model-estimated tissue-level brain peak responses directly with injury thresholds established from *in vivo* and *in vitro* micro-scale injury studies to assess the risk of injury,^{1,37} the pcBRA potentially offers a unique capability to efficiently design and evaluate the utility of injury risk metrics based on regional tissue-level responses as opposed to solely depending on global kinematic variables or their variants (e.g., GAMBIT,³⁹ HIP,⁴⁰ HITsp,¹⁷ RIC and

PRHIC,²⁶ and BrIC).⁴⁸ These findings suggest that the pcBRA does indeed have the potential to accelerate the exploration of the biomechanical mechanisms of traumatic brain injury in the future. Because brain strain-related responses, including strain itself, are significantly correlated to the product of d_{rot}^p and Δt instead to d_{rot}^p only,²⁵ a systematic investigation of how best to parameterize real-world a_{rot} impulses must be performed in the future to ensure accurate representation of brain strain responses. Interestingly, our simple parameterization strategy by maintaining both the identical v_{rot}^p and Δt from the major a_{rot} peak as outlined in Fig. 6 appeared to perform sufficiently well for the two independently measured real-world a_{rot} resultant profiles (albeit, further work is necessary to verify its utility in real-world full-DOF head rotations).

Besides the pcBRA accuracy and efficiency performances, the ultimate utility of the technique for real-world injury studies also relies on model simulation fidelity because the response approximation function, F_1 in Eq. 3, is model-dependent. The DHIM validation performance has been categorized as “good” to nearly “excellent” when simulating relative brain-skull displacements and pressure responses in cadaveric head impacts according to a fidelity rating based on correlation scores.^{24,25,60} Further, DHIM also achieved an

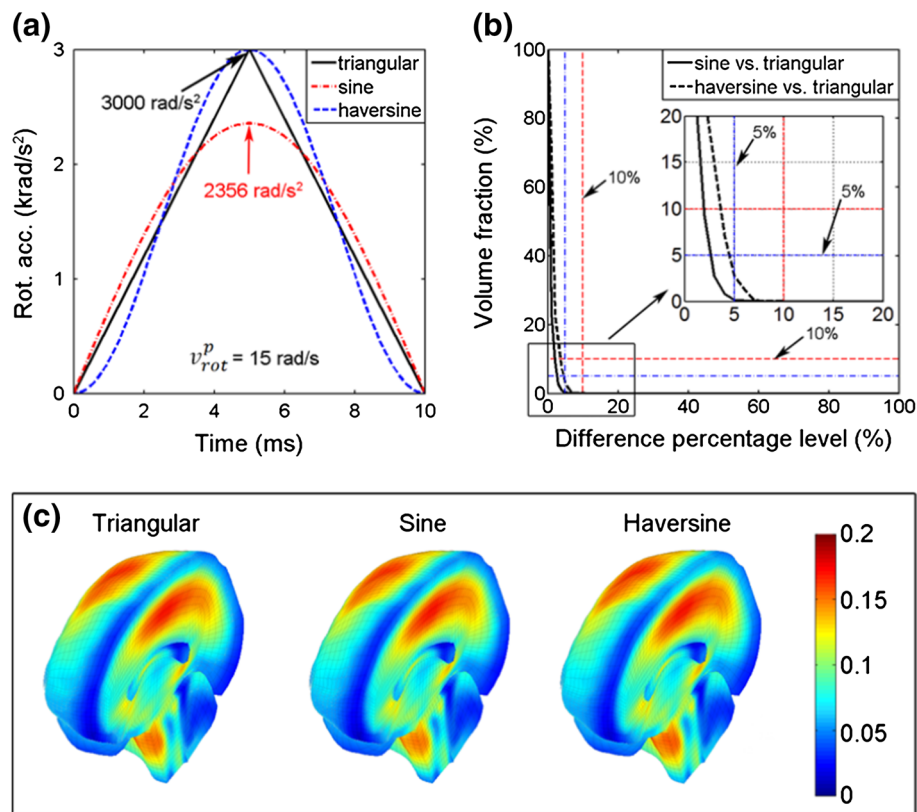


FIGURE 14. (a) Illustration of a triangular, a sine, and a haversine \mathbf{a}_{rot} impulse with an identical v_{rot}^p and Δt . (b) Volume fractions for element-wise v^p differences relative to that from the triangular impulse. (c) Comparison of the v^p distributions from the three impulses. The sine impulse had an a_{rot}^p 21.5% lower than that of the others.

“excellent” performance when validating against full-field brain strain responses in a live human (as opposed to discrete displacement data in cadavers) under a mild head rotational acceleration based on correlation scores.⁴⁷ These model response verifications at the low ($\sim 250\text{--}300 \text{ rad/s}^2$ for a volunteer), mid ($\sim 1.9\text{--}2.3 \text{ krad/s}^2$ for cadaveric impact tests C755-T2 and C383-T1), and high ($\sim 11.9 \text{ krad/s}^2$ for test C393-T4) levels of a_{rot}^p provide important insight on the confidence in DHIM-estimated regional brain strain responses for a large spectrum of on-field impacts.

The range of a_{rot}^p evaluated for pcBRA estimation performance in this study was sufficiently large (500–7500 rad/s^2 , approximately from the 25th percentile subconcussive to 95th percentile concussive a_{rot}^p in college football, or up to ~ 99 th percentile in ice-hockey; Fig. 4). We have limited the a_{rot}^p sampling range in this study to evaluate the pcBRA extrapolation accuracy at higher a_{rot}^p levels, which is important for its performance characterization. However, due to the reduced extrapolation accuracy when a_{rot}^p was sufficiently high (e.g., $> 5500 \text{ rad/s}^2$), arguably it may be necessary to further extend the range of a_{rot}^p in the training dataset to improve the pcBRA estimation accuracy (i.e., to avoid extrapolation). On the other hand, it may actually be

computationally more sensible to simply simulate the few high a_{rot}^p impulses directly instead because of the skewed distribution of on-field a_{rot}^p ,^{7,43} unless a (near) real-time feedback is critical (e.g., when possibly using the model-estimated responses to aid the “return-to-play” decision-making on the field). Although Δt was based on measured \mathbf{a}_{lin} instead of \mathbf{a}_{rot} , the temporal characteristics of the two acceleration components are likely similar,¹⁰ and the training dataset covered a large range of occurrences ($\sim 95.4\%$ assuming a normal distribution). The azimuth and elevation angles, θ and α , were also limited in this study, which can be easily extended to cover the entire parametric space for the rotational axis, Ω (Fig. 3). Because on-field data distribution of Ω is likely clustered instead of being random or uniformly distributed (e.g., see for head impact locations in Breedlove *et al.*,⁶ although on-field distribution of Ω appears not available yet), sampling the Ω parametric space accordingly will likely be more economical in computation than a simple brute-force approach. Further, the accuracy of pcBRA estimation apparently depends on the sampling density of each parameterization variable; however, we did not investigate their individual significance on the pcBRA performance. Regardless, extending the partially estab-

lished pcBRA to increase the parametric coverage space or sampling resolution for any of the independent variables is straightforward.

While we have only evaluated pcBRA performance for engineering strain in this study, the technique would most likely be applicable as well to other strains (e.g., Lagrangian or logarithmic strain), strain components (e.g., white matter fiber strain,²⁴ or alternatively, referred to as “axonal strain”),^{12,14,30,56} or strain-related responses such as strain rate and stress. Because the pcBRA model inputs were generated using generic kinematic variables that do not rely on the specific technique used in actual impact measurement (e.g., through laboratory reconstruction, instrumented helmet, mouthguard, or ATD),^{10,17,41} the pcBRA is applicable as long as it remains feasible to parameterize the isolated \mathbf{a}_{rot} profile into a triangular impulse to estimate brain strain responses. In addition, once fully established, the pcBRA could also serve as an efficient engine to conduct parametric studies, for example, to investigate the distribution and extent of potential white matter damage using randomly generated rotational impulses based on the distribution of actual on-field impact measurements.²⁴ These investigations will be the subjects of future publications.

Finally, an analogous brain pressure response atlas can also be established. Because brain pressure responses in a translational/direct head impact are causally determined by \mathbf{a}_{lin} itself (magnitude and directionality), brain size and shape,⁶⁰ only two (as opposed to four for the strain response atlas in this study) independent variables (i.e., the azimuth and elevation angles, θ and α , for the translational axis) are necessary. However, further study is necessary to assess whether pressure can be estimated from isolated \mathbf{a}_{lin} , alone, without significant loss of accuracy. Nevertheless, it may be necessary to ultimately combine these brain response atlases to fully capture the potential risk of brain injury induced by either \mathbf{a}_{lin} , \mathbf{a}_{rot} , or their combination for practical applications,⁴⁴ especially given the rather low correlation found between the two acceleration components that suggests impacts with low \mathbf{a}_{rot} but high \mathbf{a}_{lin} magnitudes are possible on the field.⁴³ These atlases designed for (near) real-time tissue-level estimation of both strain and pressure responses may provide the computational tools necessary and critical to accelerate the exploration of the biomechanical mechanisms of traumatic brain injury (including, but not limited to, sports-related concussion) in the future.

CONCLUSION

We have successfully demonstrated the feasibility of using a pre-computed brain response atlas (pcBRA) to substantially increase the efficiency in head impact

simulation for brain strain responses without significant loss of accuracy from the estimation itself using idealized, parameterized rotational impulses as well as two typical real-world rotational profiles. The typical computational cost of pcBRA was 6 s and <0.01 s for element-wise or average regional peak responses, respectively, vs. ~ 50 min simulating a 40 ms impulse directly. Future studies include systematic investigation of rotational profile parameterization and more extensive performance evaluation using real-world data. Once fully established, the pcBRA could have the potential to accelerate the exploration of the mechanisms of brain injury (sports-related concussion in particular) in the future. If successful, the pcBRA may also become a diagnostic adjunct in conjunction with sensors that measure head impact kinematics on the field to objectively monitor and identify tissue-level brain trauma in real-time for “return-to-play” decision-making on the sideline.

ACKNOWLEDGMENTS

This work was sponsored, in part, by the NIH Grant R21 NS078607 and the Dartmouth Hitchcock Foundation.

DISCLOSURE

No competing financial interests exist.

REFERENCES

- ¹Bain, A., and D. Meaney. Tissue-level thresholds for axonal damage in an experimental model of central nervous system white matter injury. *J. Biomech. Eng.* 122:615–622, 2000.
- ²Bazarian, J. J., T. Zhu, B. Blyth, A. Borrino, and J. Zhong. Subject-specific changes in brain white matter on diffusion tensor imaging after sports-related concussion. *Magn. Reson. Imaging* 30:171–180, 2012.
- ³Beckwith, J. G., R. M. Greenwald, J. J. Chu, J. J. Crisco, S. Rowson, S. M. Duma, S. P. Broglio, T. W. McAllister, K. M. Guskiewicz, J. P. Mihalik, S. Anderson, B. Schnebel, P. G. Brolinson, and M. W. Collins. Timing of concussion diagnosis is related to head impact exposure prior to injury. *Med. Sci. Sports Exerc.* 45:747–754, 2013.
- ⁴Beckwith, J. G., R. M. Greenwald, J. J. Chu, J. J. Crisco, S. Rowson, S. M. Duma, S. P. Broglio, T. W. McAllister, K. M. Guskiewicz, J. P. Mihalik, S. Anderson, B. Schnebel, P. G. Brolinson, and M. W. Collins. Head impact exposure sustained by football players on days of diagnosed concussion. *Med. Sci. Sports Exerc.* 45:737–746, 2013.
- ⁵Brainard, L. L., J. G. Beckwith, J. J. Chu, J. J. Crisco, T. W. McAllister, A.-C. Duhaime, A. C. Maerlender, and R. M. Greenwald. Gender differences in head impacts sus-

- tained by collegiate ice hockey players. *Med. Sci. Sports Exerc.* 44:297–304, 2012.
- ⁶Breedlove, E. L., M. Robinson, T. M. Talavage, K. E. Morigaki, U. Yoruk, K. O'Keefe, J. King, L. J. Leverenz, J. W. Gilger, and E. A. Nauman. Biomechanical correlates of symptomatic and asymptomatic neurophysiological impairment in high school football. *J. Biomech.* 45:1265–1272, 2012.
- ⁷Broglio, S. P., T. Surma, and J. A. Ashton-Miller. High school and collegiate football athlete concussions: a biomechanical review. *Ann. Biomed. Eng.* 40:37–46, 2012.
- ⁸Broglio, S. P., B. Schnebel, J. J. Sosnoff, S. Shin, X. Fend, X. He, and J. Zimmerman. Biomechanical properties of concussions in high school football. *Med. Sci. Sports Exerc.* 42:2064–2071, 2010.
- ⁹Broglio, S. P., J. J. Sosnoff, S. Shin, X. He, C. Alcaraz, and J. Zimmerman. Head impacts during high school football: a biomechanical assessment. *J. Athl. Train.* 44:342–349, 2009.
- ¹⁰Camarillo, D. B., P. B. Shull, J. Mattson, R. Shultz, and D. Garza. An instrumented mouthguard for measuring linear and angular head impact kinematics in American football. *Ann. Biomed. Eng.* 41:1939–1949, 2013.
- ¹¹Centers for Disease Control and Prevention. Report to congress on mild traumatic brain injury in the United States: steps to prevent a serious public health problem. GA: Atlanta, 2003.
- ¹²Chatelin, S., C. Deck, F. Renard, S. Kremer, C. Heinrich, J.-P. Armspach, and R. Willinger. Computation of axonal elongation in head trauma finite element simulation. *J. Mech. Behav. Biomed. Mater.* 4:1905–1919, 2011.
- ¹³Chen, Y., and M. Ostojca-Starzewski. MRI-based finite element modeling of head trauma: spherically focusing shear waves. *Acta Mech.* 213:155–167, 2010.
- ¹⁴Cloots, R. J. H., J. A. W. van Dommelen, T. Nyberg, S. Kleiven, and M. G. D. Geers. Micromechanics of diffuse axonal injury: influence of axonal orientation and anisotropy. *Biomech. Model. Mechanobiol.* 10:413–22, 2011.
- ¹⁵Crisco, J. J., R. Fiore, J. G. Beckwith, J. J. Chu, P. G. Brolinson, S. Duma, T. W. McAllister, A.-C. Duhaim, and R. M. Greenwald. Frequency and location of head impact exposures in individual collegiate football players. *J. Athl. Train.* 45:549–559, 2010.
- ¹⁶Dumpuri, P., R. C. Thompson, B. M. Dawant, A. Cao, and M. I. Miga. An atlas-based method to compensate for brain shift: preliminary results. *Med. Image Anal.* 11:128–45, 2007.
- ¹⁷Greenwald, R., J. Gwin, J. Chu, and J. Crisco. Head impact severity measures for evaluating mild traumatic brain injury risk exposure. *Neurosurgery* 62:789–798, 2008.
- ¹⁸Hakopian, H. Multivariate spline functions, B-spline basis and polynomial interpolations. *SIAM J. Numer. Anal.* 19:510–517, 1982.
- ¹⁹Hardy, W. N., C. D. Foster, M. J. Mason, K. H. Yang, A. I. King, and S. Tashman. Investigation of head injury mechanisms using neutral density technology and high-speed biplanar X-ray. *Stapp Car Crash J.* 45:337–368, 2001.
- ²⁰Hardy, W. N., M. J. Mason, C. D. Foster, C. S. Shah, J. M. Kopacz, K. H. Yang, A. I. King, J. Bishop, M. Bey, W. Anderst, and S. Tashman. *A Study of the Response of the Human Cadaver Head to Impact.* 51:17–80, 2007.
- ²¹Holbourn, A. The mechanics of brain injuries. *Lancet* 2:438–441, 1943.
- ²²Ji, S., J. C. Ford, R. M. Greenwald, J. G. Beckwith, K. D. Paulsen, L. A. Flashman, and T. W. McAllister. Automated subject-specific, hexahedral mesh generation via image registration. *Finite Elem. Anal. Des.* 47:1178–1185, 2011.
- ²³Ji, S., H. Ghadyani, R. P. Bolander, J. G. Beckwith, J. C. Ford, T. W. McAllister, L. A. Flashman, K. D. Paulsen, K. Ernstrom, S. Jain, R. Raman, L. Zhang, and R. M. Greenwald. Parametric comparisons of intracranial mechanical responses from three validated finite element models of the human head. *Ann. Biomed. Eng.* 42:11–24, 2014.
- ²⁴Ji, S., W. Zhao, J. C. Ford, J. G. Beckwith, R. P. Bolander, R. M. Greenwald, L. A. Flashman, K. D. Paulsen, and T. W. McAllister. Group-wise evaluation and comparison of white matter fiber strain and maximum principal strain in sports-related concussion. *J. Neurotrauma* 2014. doi: 10.1089/neu.2013.3268.
- ²⁵Ji, S., W. Zhao, Z. Li, and T. W. McAllister. Head impact accelerations for brain strain-related responses in contact sports: a model-based investigation. *Biomech. Model. Mechanobiol.* 13:1121–1136, 2014.
- ²⁶Kimpara, H., and M. Iwamoto. Mild traumatic brain injury predictors based on angular accelerations during impacts. *Ann. Biomed. Eng.* 40:114–126, 2012.
- ²⁷King, A., K. Yang, and L. Zhang. Is head injury caused by linear or angular acceleration. 2003.
- ²⁸Kleiven, S. Evaluation of head injury criteria using a finite element model validated against experiments on localized brain motion, intracerebral acceleration, and intracranial pressure. *Int. J. Crashworthiness* 11:65–79, 2006.
- ²⁹Kleiven, S. Predictors for traumatic brain injuries evaluated through accident reconstructions. *Stapp Car Crash J.* 51:81–114, 2007.
- ³⁰Kraft, R. H., P. J. McKee, A. M. Dagro, and S. T. Graf-ton. Combining the finite element method with structural connectome-based analysis for modeling neurotrauma: connectome neurotrauma mechanics. *PLoS Comput. Biol.* 8:e1002619, 2012.
- ³¹Loader, C. Local Regression and Likelihood. New York: Springer, 1999.
- ³²Marjoux, D., D. Baumgartner, and C. Deck. Head injury prediction capability of the HIC. *HIP, SIMon and ULP criteria.* 40:1135–1148, 2008.
- ³³McAllister, T. W., J. C. Ford, L. A. Flashman, A. Maerlender, R. M. Greenwald, J. G. Beckwith, R. P. Bolander, T. D. Tosteson, J. H. Turco, R. Raman, and S. Jain. Effect of head impacts on diffusivity measures in a cohort of collegiate contact sport athletes. *Neurology* 82:63–69, 2014.
- ³⁴McAllister, T. W., J. C. Ford, S. Ji, J. G. Beckwith, L. A. Flashman, K. Paulsen, and R. M. Greenwald. Maximum principal strain and strain rate associated with concussion diagnosis correlates with changes in corpus callosum white matter indices. *Ann. Biomed. Eng.* 40:127–140, 2012.
- ³⁵McCrea, M., T. Hammeke, G. Olsen, P. Leo, and K. M. Guskiewicz. Unreported concussion in high school football players. *Clin. J. Sport Med.* 14:385; author reply 385, 2004.
- ³⁶McKee, A., R. Cantu, C. Nowinski, E. Hedley-Whyte, B. Gavett, A. Budson, V. Santini, H. Lee, C. Kubilus, and R. Stern. Chronic traumatic encephalopathy in athletes: progressive tauopathy following repetitive head injury. *J. Neuropathol. Exp. Neurol.* 68:709–735, 2009.
- ³⁷Morrison, B. III, D. Cullen, and M. LaPlaca. In vitro models for biomechanical studies of neural tissues. *Neural Tissue Biomech. Stud. Mechanobiol. Tissue Eng. Biomater.* 3:247–285, 2011.

- ³⁸Nahum, A., R. Smith, and C. Ward. Intracranial pressure dynamics during head impact. *SAE Tech. Pap.* No. 770922, 1977.
- ³⁹Newman, J. A generalized acceleration model for brain injury threshold (GAMBIT). 1986.
- ⁴⁰Newman, J., and N. Shewchenko. A proposed new biomechanical head injury assessment function-the maximum power index. *Stapp Car Crash J.* 44:215–247, 2000.
- ⁴¹Pellman, E. J., D. C. Viano, A. M. Tucker, I. R. Casson, and J. F. Waeckerle. Concussion in professional football: reconstruction of game impacts and injuries. *Neurosurgery* 53:799–814, 2003.
- ⁴²Post, A., B. Hoshizaki, and M. D. Gilchrist. Finite element analysis of the effect of loading curve shape on brain injury predictors. *J. Biomech.* 45:679–683, 2012.
- ⁴³Rowson, S., G. Brolinson, M. Goforth, D. Dietter, and S. Duma. Linear and angular head acceleration measurements in collegiate football. *J. Biomech. Eng.* 131:061016, 2009.
- ⁴⁴Rowson, S., and S. M. Duma. Brain injury prediction: assessing the combined probability of concussion using linear and rotational head acceleration. *Ann. Biomed. Eng.* 41:873–882, 2013.
- ⁴⁵Rowson, S., S. M. Duma, J. G. Beckwith, J. J. Chu, R. M. Greenwald, J. J. Crisco, P. G. Brolinson, A.-C. Duhaime, T. W. McAllister, and A. C. Maerlender. Rotational head kinematics in football impacts: an injury risk function for concussion. *Ann. Biomed. Eng.* 40:1–13, 2012.
- ⁴⁶Rowson, S., J. G. Beckwith, J. J. Chu, D. S. Leonard, R. M. Greenwald, and S. M. Duma. A six degree of freedom head acceleration measurement device for use in football. 8–14, 2011.
- ⁴⁷Sabet, A. A., E. Christoforou, B. Zatlin, G. M. Genin, and P. V. Bayly. Deformation of the human brain induced by mild angular head acceleration. *J. Biomech.* 41:307–315, 2008.
- ⁴⁸Takhounts, E. G., M. J. Craig, K. Moorhouse, J. McFadden, and V. Hasija. Development of brain injury criteria (Br IC). *Stapp Car Crash J.* 57:243–266, 2013.
- ⁴⁹Takhounts, E. G., S. A. Ridella, R. E. Tannous, J. Q. Campbell, D. Malone, K. Danelson, J. Stitzel, S. Rowson, and S. Duma. Investigation of traumatic brain injuries using the next generation of simulated injury monitor (SI-Mon). *Finite Element Head Model.* 52:1–31, 2008.
- ⁵⁰Talavage, T. M., E. A. Nauman, E. L. Breedlove, U. Yoruk, A. E. Dye, K. E. Morigaki, H. Feuer, and L. J. Leverenz. Functionally-detected cognitive impairment in high school football players without clinically-diagnosed concussion. *J. Neurotrauma* 12:1–12, 2013.
- ⁵¹Trosseille, X., C. Tarriere, F. Lavaste, F. Guillon, and A. Domont. Development of a FEM of the human head according to a specific test protocol. 1992.
- ⁵²Urban, J. E., E. M. Davenport, A. J. Golman, J. A. Maldjian, C. T. Whitlow, A. K. Powers, and J. D. Stitzel. Head impact exposure in youth football: high school ages 14 to 18 years and cumulative impact analysis. *Ann. Biomed. Eng.* 41:2474–2487, 2013.
- ⁵³van Dommelen, J. A. W., T. P. J. van der Sande, M. Hrapko, and G. W. M. Peters. Mechanical properties of brain tissue by indentation: interregional variation. *J. Mech. Behav. Biomed. Mater.* 3:158–166, 2010.
- ⁵⁴Weaver, A. A., K. A. Danelson, and J. D. Stitzel. Modeling brain injury response for rotational velocities of varying directions and magnitudes. *Ann. Biomed. Eng.* 40:2005–2018, 2012.
- ⁵⁵Willinger, R., and D. Baumgartner. Numerical and physical modelling of the human head under impact-towards new injury criteria. *Int. J. Veh. Des.* 32:94–115, 2003.
- ⁵⁶Wright, R. M., A. Post, B. Hoshizaki, and K. T. Ramesh. A multiscale computational approach to estimating axonal damage under inertial loading of the head. *J. Neurotrauma* 30:102–118, 2013.
- ⁵⁷Yang, K., H. Mao, C. Wagner, F. Zhu, C. C. Chou, and A. I. King. Modeling of the brain for injury prevention. In: *Studies in Mechanobiology, Tissue Engineering and Biomaterials*. Berlin: Springer-Verlag, pp. 69–120, 2011 at <http://www.springerlink.com/index/U7368378332M5820.pdf>.
- ⁵⁸Yoganandan, N., J. Li, J. Zhang, F. A. Pintar, and T. A. Gennarelli. Influence of angular acceleration-deceleration pulse shapes on regional brain strains. *J. Biomech.* 41:2253–2262, 2008.
- ⁵⁹Zhang, L., K. H. Yang, and A. I. King. A proposed injury threshold for mild traumatic brain injury. *J. Biomech. Eng.* 126, 2004.
- ⁶⁰Zhao, W., S. Ruan, and S. Ji. Brain pressure responses in translational head impact: a dimensional analysis and a further computational study. *Biomech. Model. Mechanobiol.* 2014. doi: [10.1007/s10237-014-0634-0](https://doi.org/10.1007/s10237-014-0634-0).